machines

MDPI

Article

The Deformation Mechanism of the Rings of Angular-Contact Ball Bearings During the Quenching and Tempering Process

Ruijie Gu, Yi Tong, Qiang Wang *, Liaoyuan Chen and Ziyang Shang

School of Mechatronics Engineering, Henan University of Science and Technology, Luoyang 471003, China; iapte@haust.edu.cn (R.G.); 220320010098@stu.haust.edu.cn (Y.T.); lychen8790@haust.edu.cn (L.C.); 230320010143@stu.haust.edu.cn (Z.S.)

* Correspondence: wangq0911@haust.edu.cn

Abstract: During the heat treatment process, bearing rings are subjected to drastic temperature variability and complex microstructural evolution, which result in deformation, high residual stresses, operational instability and a limited operating life. However, the underlying relationship between temperature, phase transformation, and deformation has not been fully revealed in previous research. As a result, it is difficult to accurately control the roundness of bearing rings during the heat treatment process. Therefore, a combination of numerical simulations and experimental methods was employed to analyze the heat treatment process of the rings of angular-contact ball bearings (ACBB) (7008C). Firstly, according to the multiple coupling theory of thermal, phase-transition, and stress–strain fields, a model for the numerical simulation of the quenching and tempering process was established. Secondly, the thermal–physical properties of the material were calculated using the Jmatpro 7.0 software, and the quenching and tempering processes were numerically simulated using the Deform software. Subsequently, the evolution of the stress, phase-transformation, and deformation behaviors of bearing rings during the quenching and tempering were studied in detail. Finally, the roundness errors of the bearing rings were obtained by a coordinate-measuring machine (CMM). The results showed that the axial and radial stress distributions at the surface and center of the bearing rings were significantly different. The bearing rings experienced uneven expansion and deformation. The roundness errors of the inner diameter and outer diameter of the inner ring were 0.0386 mm and 0.0423 mm, respectively. The roundness errors of the inner diameter and outer diameter of the outer ring were 0.0202 mm and 0.0180 mm, respectively. In this study, the mechanism of the effect of the temperature variation and phase transformation on deformation during the quenching and tempering process was revealed in detail. This provides a reference for controlling the roundness of bearing rings in actual production processes.

Keywords: angular-contact ball bearings; bearing rings; deformation; roundness error

check for updates

Academic Editor: Kai Cheng

Received: 18 December 2024
Revised: 13 January 2025
Accepted: 14 January 2025
Published: 17 January 2025

Citation: Gu, R.; Tong, Y.; Wang, Q.; Chen, L.; Shang, Z. The Deformation Mechanism of the Rings of Angular -Contact Ball Bearings During the Quenching and Tempering Process. *Machines* **2025**, *13*, 64. https://doi.org/10.3390/machines13010064

Copyright: © 2025 by the authors. Licensee MDPI, Basel, Switzerland. This article is an open access article distributed under the terms and conditions of the Creative Commons Attribution (CC BY) license (https://creativecommons.org/licenses/by/4.0/).

1. Introduction

Rolling bearings are critical components in mechanical drive systems and are commonly applied in a wide range of industrial devices, such as aerospace, automotive, and precision instruments. Their main function is to support loads and reduce friction to improve motion efficiency and extend service life. However, with changing working conditions and increasing loads, rolling bearings will encounter a series of frictional failures during long-term use, and the most common problems include wear and tear, fatigue, overheating, and poor lubrication. In particular, when bearings are subjected to high loads, high speeds, or harsh environmental conditions, the high temperatures generated by friction

can lead to premature bearing failure [1]. The challenges posed to the stability and safety of the equipment are enormous. Thermal diagnostics play a vital role during the operation of bearings. The stable thermal conductivity of bearing components directly affects their thermal conductivity, which, in turn, affects the operating temperature distribution and operational performance of the bearing. By analyzing the temperature distribution of bearings under different operating conditions through simulations, the thermal state of the bearings can be predicted, and failures due to overheating in the friction area can also be prevented [2,3]. In addition, the temperature conditions of bearings are closely related to their tribological performance. Excessive temperatures not only accelerate the deterioration of the lubricant but may also lead to thermal deformation or the phase transformation of the bearing material. This will affect its load-bearing capacity and service life.

To solve this problem, the heat treatment of bearings becomes an important means to optimize their performance and extend their service life. Through the reasonable design and optimization of the bearing heat treatment process, the bearing's surface hardness, wear resistance, and fatigue resistance will be effectively enhanced, thus reducing the occurrence of tribological failures. In addition, the hardness and wear resistance of bearing rings can be significantly increased by the quenching and tempering process [4,5]. However, due to the rapid temperature changes that occur during the process of quenching, the various positions of the bearing rings may be cooled unevenly, and the phase-transition time at each position may be inconsistent. Then, uneven thermal and phase-transition stresses will be generated, and the bearing rings will be distorted [6–8]. Consequently, it is important to explore the stress evolution and phase-transformation mechanism during quenching and tempering processes and to grasp the mechanism of their effects on the deformation of bearing rings.

To control the deformation of key components during the heat treatment process, a lot of research has been carried out by many scholars into the optimization of the heat treatment process parameters. To ensure deformation precision, the deformation behavior of SAE 5160 steel at different cooling rates was investigated by Lopez-Garcia [9]. The study revealed that heat treatment deformation can be effectively controlled at an appropriate cooling rate. Afterwards, the thermophysical and mechanical properties of the material were obtained by Lopez-Garcia [10], and finite-element software was applied to study the impact of different quenching parameters on the deformation of the quenched components. To reduce the deformation generated in the heat treatment process of helical gears, the temperature, phase transformations, and axial stresses during the process were studied by Kim [11], and the deformation of the gears was effectively reduced by optimizing the cooling temperatures. To address problems such as the large deformation of the ring diameter during the heat treatment of bearing rings, the effects of the cold treatment process on the roundness of the ring raceway were studied by Shao et al. [12]. The effect of a die on gear quenching deformation was analyzed by Liu et al. [13], and it was found that the inner hole die could effectively limit the radial shrinkage deformation of the gears. The development of numerical simulation technology has enabled it to become an effective method for studying the deformation behavior of the heat treatment process. Vacuum oil quenching multi-field coupling simulation was used by Liu et al. [14], and it was found that the quenching oil temperature has little effect on the deformation, while the pressure above the quenching tank has a greater effect on the deformation. The mechanism of ellipticity distortion during the quenching process of the bearing rings was revealed by Li [15] through a combination of simulations and experiments. To improve the accuracy of the simulation results for the volume change during the quenching process, a bainite phase transformation kinetics model was introduced into the simulation by Esfahani et al. [16]. A carburizing and quenching model of the gear ring was established by Wang et al. [17], and the deformation

mechanism of gears was analyzed based on the carburizing layer and phase transformation results. The carburizing and quenching process parameters were optimized through orthogonal experiments. By setting different thermal boundary conditions on the bearing rings, the elliptical deformation behavior of bearing rings after the heat treatment process was studied by Liu et al. [18]. It has been shown that heat treatment deformation is not only related to the instantaneous temperature, but also affected by the phase transformation and other factors. The material parameters related to deformation during the quenching process were analyzed by Chen et al. [19], and it was found that the phase transition temperature and quenching temperature have a significant effect on quenching deformation. Taking into account the effects of cooling rate and solid-phase phase transformation on stresses and deformations, the stresses and deformations of AF1410 steel in three quenching mediums (water quenching, oil quenching and vacuum gas quenching) were studied by Zhang et al. [20]. The behavior of the phase transformation and deformation of carburized C-ring during the cooling period was analyzed by Yan et al. [21], and the mechanism of interaction between the phase transformation and deformation during the carburizing and quenching process of gear steel was revealed.

In summary, extensive research on the heat treatment deformation of components has been conducted by numerous experts. However, the shape change of the bearing rings during the heat treatment process is not only related to their dimensional structure, but also involves the coupling effect of temperature variation, phase transformation, and stress–strain interaction. In particular, the rings of ACBBs are characterized by thin cross-sections and high quenching sensitivity. It is difficult to accurately describe the deformation during the heat treatment process. Therefore, numerical simulation and experimentation were adopted in this paper, and the mechanism of the effect of temperature variation and phase transformation on the deformation of the rings of ACBBs (7008C) during quenching and tempering processes was studied. To more accurately simulate the deformation behavior of bearing rings during quenching and tempering, a numerical model with multi-physics field coupling was adopted in this paper. The coupling effects of multiple physical fields, including heat, mechanics, and phase transformation, were comprehensively considered. The refined thermal–force coupling simulation provides a better description of the stress distribution induced by temperature gradients and the local deformation of thin-walled structures. Due to the significant deformation of thin-walled bearing rings during the heat treatment process, conventional uniform meshes may not provide sufficient computational accuracy in critical areas, such as deformation zones and regions with large temperature gradients. To improve computational accuracy while maintaining computational efficiency, the adaptive mesh technique is introduced to automatically refine the mesh in regions of more severe deformation. The simulation of the cooling rate during the heat treatment process is optimized for the special geometry of thin-walled bearing rings. The heat transfer process between the cooling medium and the surface of the workpiece is combined. It accurately describes the conduction and convection of heat and avoids the error caused by the inaccurate cooling rate in the traditional method. Finally, the roundness error of the heat-treated bearing rings was measured by a coordinate-measuring machine (CMM) to verify the simulation results.

The aim of this study was to reveal the deformation mechanism during the quenching and tempering of bearing rings, providing a basis for controlling the roundness accuracy of shaped thin-section bearing rings to ensure the machining quality.

2. Numerical Model

The heat treatment process involves the coupling of temperature, phase-transformation, stress and strain in a multi-field interaction. The heat treatment multi-field coupling

schematic is shown in Figure 1. Temperature changes generate thermal stresses; these stresses induce phase transformation; and the phase transformations absorb or release heat due to the latent heat of phase transformation. The temperature changes can also induce phase transformation. The phase transformations also cause stresses and deformations, and heat is generated by the deformations.

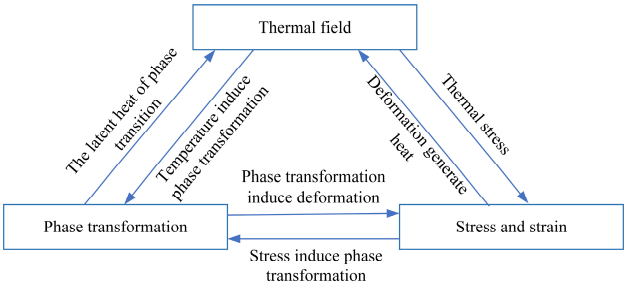


Figure 1. The heat treatment multi-field coupling schematic.

During the simulation of the heat treatment of bearing rings, complex physical phenomena such as deformation, stress and phase transformation need to be effectively calculated and analyzed. Some of the problems are simplified idealized in this paper.

1. Firstly, the material's constitutive relationship uses a simplified model to describe the mechanical behavior of the steel. This model disregards the evolution of microstructure and the anisotropy of materials to reduce computational complexity.
2. Secondly, the bearing ring undergoes uniform heat transfer during the heat conduction process. Furthermore, potential material heterogeneity and detail are disregarded.
3. Although the microstructure of the material (e.g., grain size, carbon content, etc.) has some effect on the deformation, in order to focus on the main deformation mechanisms of the heat treatment process, the effect of these microscopic factors is disregarded for the time being.
4. In addition, although the temperature distribution and phase transformation behavior during the heat treatment process are more complex, based on a large number of experimental studies, the phase transformation properties of steel are described using a simplified model in order to obtain effective results within a reasonable computational time and using a reasonable number of resources.

The main purpose of these simplifications and idealizations is to reduce the complexity of the simulation calculations. This ensures that problems such as deformation, residual stresses, and phase transformation during the heat treatment process can be accurately assessed at this stage, laying the foundation for further research in the future.

2.1. Geometric Model

The geometric structures of the rings of ACBBs (7008C) selected for this paper are shown in Figure 2. The geometry of the inner ring is shown in Figure 2a, where B is 15 mm, d is 40 mm, d_1 is 40.8 mm and d_2 is 50.4 mm. The geometry of the outer ring is shown in Figure 2b, where D is 68 mm, and D_1 is 58.08 mm.

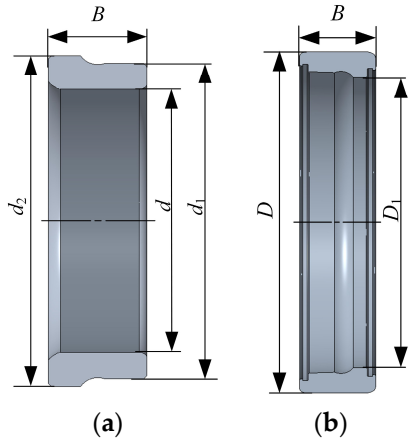


Figure 2. The geometric structures of the bearing rings: (**a**) inner ring; (**b**) outer ring.

2.2. Setup for the Model Solution

The heat treatment process of bearing rings was numerically simulated using Deform 10.2 software. Considering that the bearing rings are not completely symmetrical in terms of deformation during the actual production process, the overall model was chosen as the simulation object. During the actual production of bearing rings, the quenching and tempering processes are carried out after the annealing process. The internal microstructure of the annealed bearing rings is mostly pearlite. Therefore, the initial microstructure of the bearing rings was defined as pearlite with an initial hardness of 30 HRC, and the initial temperature was 25 °C. Ordinary quenching oil was used as the quenching media during the quenching process of bearing rings. The heat transfer coefficients between it and the bearing rings [22] are shown in Table 1.

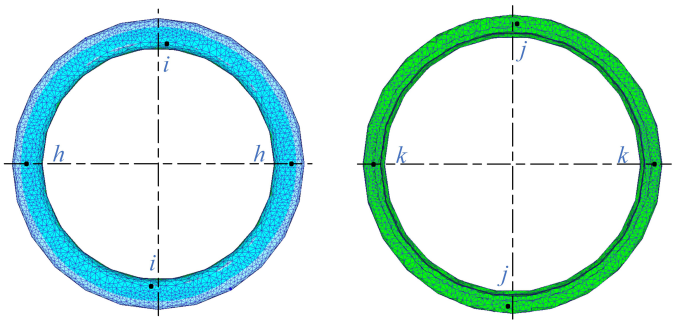
Table 1. The heat transfer coefficient of quenching oil.

T (°C)	25	100	200	300	400	500	600	700	800	900
HTC ($kW/m^2{}^\circ C$)	0.02	0.035	0.289	0.464	0.921	1.238	1.834	1.485	1.107	0.565

The mesh and constraint boundary condition settings are shown in Figure 3. To deal with complex deformation and temperature fields, adaptive mesh techniques were used. The inner and outer rings were meshed using tetrahedral mesh elements, and the mesh size and solution details were set as shown in Table 2. The schematic diagram of the fixed node of the inner ring is shown in Figure 3a. Node *i* indicates that the degrees of freedom of the inner ring are constrained in the *X* and *Y* directions. Node *h* indicates that the degrees of freedom of the inner ring in the *X* and *Z* directions are constrained. The schematic diagram of the fixed node of the outer ring is shown in Figure 3b. Node *j* indicates that the degrees of freedom of the outer ring in the *X* and *Y* directions are constrained. Node *k* indicates that the degrees of freedom of the outer ring in the *X* and *Z* directions are constrained.

Table 2. Parameters set for numerical simulation.

Parameters	Inner Ring	Outer Ring
The total number of simulated steps	3824	3875
The number of elements	69,984	56,768
The minimum element size	0.555 mm	0.74 mm
The maximum element size	1.110 mm	1.48 mm
The temperature increment per step	2	2
Room temperature	25 °C	



(**a**) (**b**)

Figure 3. The schematic diagram of mesh and fixed nodes: (**a**) inner ring; (**b**) outer ring.

2.3. Governing Equations

The quenching process of the bearing rings involves three heat transfer methods: thermal conduction, thermal radiation, and thermal convection. Since thermal radiation does not have a significant effect on the heat loss of the bearing rings, it is not considered in the numerical simulation. Using the principle of energy conservation and Fourier's law, the governing equation for three-dimensional transient heat transfer in solids can be formulated as follows [23]:

$$qv = c_p\rho\frac{\partial T}{\partial t} - \frac{\partial}{\partial x}(k\frac{\partial T}{\partial x}) - \frac{\partial}{\partial y}(k\frac{\partial T}{\partial y}) - \frac{\partial}{\partial z}(k\frac{\partial T}{\partial z}) \quad (1)$$

where T is the temperature of the bearing rings, °C; t is the heat transfer time, s; k is the thermal conductivity, W/m·°C; ρ is the density, kg/m^3; qv is the latent heat of phase transition, J/kg; and c_p is the specific heat capacity, J/kg·°C.

The thermal interaction between the surface of the bearing ring and the cooling medium is characterized by thermal convection, which is expressed by the following [23]:

$$Q = hA\Delta T \quad (2)$$

where Q is the density of heat flux, W/m^2; h is the heat transfer coefficient, W/m^2·°C; A is the surface area of the bearing rings, m^2; and ΔT is the temperature difference between the surface of the bearing rings and the quenching oil, °C.

The transformation from pearlite to austenite during the quenching process of the bearing rings is a diffusion-type phase transformation, as given by the following [24]:

$$\omega_{\mathrm{A}} = 1 - \exp\left\{R(\frac{T - T_s}{T_e - T_s})^N\right\} \quad (3)$$

where ω_{A} is the amount of austenite transformed; T_s is the temperature at the beginning of the austenite transformation, °C; and T_e is the temperature at the end of the austenite transformation, °C; and R and N are constants. T_s is 722 °C, T_e is 816 °C, and R is −4, N is 2.

During the quenching process, the transformation from austenite to martensite in the bearing rings is a non-diffusive phase transition, as given by the following [25]:

$$\omega_{\mathrm{M}} = 1 - \exp(\psi_1 T + \psi_2) \quad (4)$$

where ω_{M} is the martensitic transformation; T is the temperature, °C; and ψ_1 and ψ_2 are martensite transformation scale factors. ψ_1 is 0.016 and ψ_2 is −5.18.

Temperature variations and phase transitions produce stresses and distortions during the quenching and tempering processes. The total strain in the material can be calculated from the linear superposition of the individual strains, as given by the following [25]:

$$d\varepsilon ij = d\varepsilon^{e}_{ij} + d\varepsilon^{p}_{ij} + d\varepsilon^{th}_{ij} + d\varepsilon^{tr}_{ij} + d\varepsilon^{tp}_{ij} \quad (5)$$

where $d\varepsilon_{ij}$ is the total strain; $d\varepsilon^{e}{}_{ij}$ is the thermoelastic strain; $d\varepsilon^{p}{}_{ij}$ is the plastic strain; $d\varepsilon^{th}{}_{ij}$ is the thermal strain; $d\varepsilon^{tr}{}_{ij}$ is the phase transformation strain; and $d\varepsilon^{tp}{}_{ij}$ is the phase transformation plastic strain.

2.4. The Material Property Parameters

GCr15 is used as the material of the rings of ACBBs (7008C). A direct-reading spectrometer (SPECTRO M12, SPECTRO Analytical Instruments, Kleve, Germany) was used to measure the content of each element in the rings, and the results are shown in Figure 4. The content of Ni, Cu, P and S and other elements met the requirements of special-grade quality steel in the relevant standards [26].

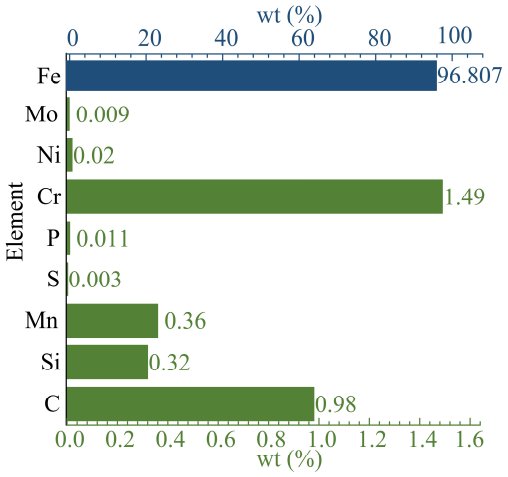


Figure 4. The content of elements in bearing rings.

The thermal property parameters of the bearing rings mainly include the density, modulus of elasticity, coefficient of thermal expansion, Poisson's ratio, specific heat capacity, and thermal conductivity. Since the thermal performance parameters of the material change with temperature, the relationship between the thermal property parameters and temperature was calculated using JmatPro 7.0 software (as shown in Table 3). In Table 3, T represents the temperature, A stands for austenite, P stands for pearlite and M stands for martensite.

Table 3. The thermal property parameters of the bearing rings.

T (°C)	Density (kg/m^3)			Modulus of Elasticity (Gpa)			Coefficient of Thermal Expansion (1/10^6 °C)			Poisson's Ratio			Specific Heat Capacity (J/kg·°C)			Thermal Conductivity (W/m·°C)		
	A	P	M	A	P	M	A	P	M	A	P	M	A	P	M	A	P	M
25	8.01	7.82	7.74	201	210	210	24.29	11.75	12.30	0.292	0.287	0.289	453	470	448	17.13	44.68	38.08
100	7.96	7.79	7.72	194	206	206	24.25	12.36	12.80	0.296	0.290	0.292	478	499	482	18.10	43.45	39.62
200	7.91	7.77	7.69	185	201	200	24.21	13.14	13.58	0.302	0.293	0.296	501	534	524	19.30	41.51	40.40
300	7.85	7.73	7.65	176	193	192	24.18	13.95	14.30	0.308	0.297	0.300	520	574	571	20.50	39.27	39.94
400	7.80	7.70	7.62	167	183	182	24.16	14.78	15.01	0.313	0.300	0.304	538	622	628	21.70	36.91	38.46
500	7.74	7.67	7.59	158	172	170	24.16	15.63	15.73	0.319	0.304	0.308	555	684	702	22.90	34.61	36.35
600	7.69	7.63	7.55	149	160	157	24.16	16.50	16.46	0.325	0.307	0.312	571	783	805	24.10	32.43	34.08
700	7.64	7.59	7.51	139	146	143	24.18	17.41	17.18	0.331	0.311	0.316	587	928	973	25.30	30.56	32.08
800	7.59	7.55	7.48	130	131	127	24.21	18.33	17.90	0.336	0.314	0.320	603	841	808	26.49	29.29	30.65
900	7.54	7.51	7.44	120	116	112	24.52	19.26	18.63	0.342	0.318	0.324	618	783	737	27.69	28.71	29.93

3. Experiment

The quenching and tempering processes for the simulation and experiment are shown in Figure 5. The bearing rings were heated to 830 °C and then held for 1 hour, after which they were cooled in quenching oil at 70 °C. The ring surfaces were cleaned after the cooling process. Finally, the bearing rings were heated to 160 °C and held for 3 h for tempering.

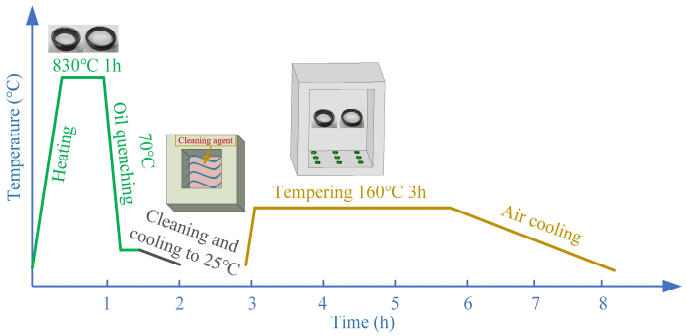


Figure 5. The quenching and tempering process of the bearing rings.

A controlled-atmosphere production line with a roller mesh belt was used as the heat treatment experimental equipment for this research. This mainly consists of the charging table, the controlled atmosphere heating furnace with roller mesh belt, the quenching oil tank, the washing sink, the heating furnace of tempering and so on (as shown in Figure 6). This equipment has a comprehensive automatic control system, including atmosphere control, temperature uniformity control, and heating and holding time control. The heat treatment quality of the bearing rings is more reliable and more closely matched to the numerical simulation.

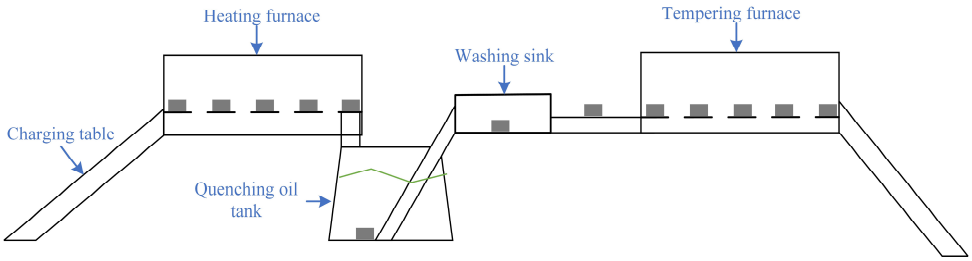


Figure 6. A schematic diagram of the controlled-atmosphere production line with the roller mesh belt.

The dimensions of the bearing rings were measured using the CMM (CONTURA G2 7/10/6RDS) manufactured by Carl Zeiss, Jena, Germany. A schematic diagram of the CMM is shown in Figure 7. Three heat-treated bearing rings were selected and measured for roundness. The average value of these measurements was taken as the experimental result.

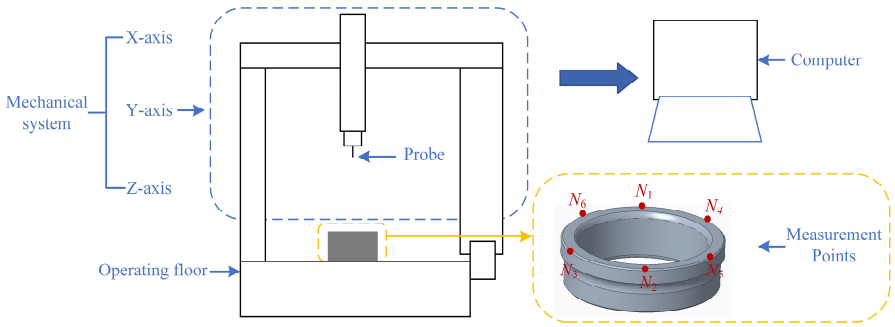


Figure 7. A schematic diagram of the CMM.

4. Results and Discussion

4.1. The Stress Evolution of the Bearing Rings During the Quenching Process

The bearing rings generate thermal stress and phase transformation stress during the quenching cooling process. These stresses interact with each other and lead to the uneven deformation of the bearing rings. Therefore, the stress evolution mechanism during the quenching process was studied, as it is crucial to reveal how these stresses affect the deformation of the bearing rings. To study the evolution of stresses in bearing rings during the quenching process, the inner ring was taken as an example. Five nodes (R1–R5) on the inner ring, as shown in Figure 8, were selected to explore the effects of temperature variations and phase transformations on the stress evolution in the inner ring.



Figure 8. A schematic diagram of the nodes.

From Figure 9a, it can be seen that the stress at points R3 and R2 on the raceway is consistently higher than that at other positions. In the initial stage of the process, the inner ring surface is the first to cool, and the stress on the surface increases. At the same time, the stress in the center also increases due to the effect of the surface compressive stress. Afterwards, the stress decreases because the center of the inner ring begins to cool, and the stress generated in the center is opposite to that on the surface. As the cooling process progresses, martensitic transformation first occurs on the outer surface of the inner ring, resulting in the expansion of the outer surface and an increase in stress. The stress then decreases as martensitic transformation occurs in the center. Once the martensitic transformation is completed, the inner ring temperature approaches that of the quenching oil, and the stress variations level off. Research by Zhu et al. [27] emphasized that the temperature gradient between the surface and the center during the quenching process is the main driver of the stress evolution. Research by Qin et al. [28] also indicated that during martensitic transformation, the stress tends to increase at the surface due to increases in the volume, while the phase transformation at the center leads to a decrease in stress. This is consistent with the findings of this paper.

As can be seen from Figure 9b–d, the axial and radial stresses have a significant effect on the variation in the effective stresses, while the circumferential stresses have little effect on the effective stresses. After the cooling of the quenching process, the axial stresses at points R1, R2 and R3 on the raceway surface of the inner ring are mainly compressive stresses. The axial stresses at point R4 in the center of the inner ring and at point R5 on the inner surface of the inner ring are tensile stresses. The tensile stresses on the inner surface of the inner ring are larger than those at the center. The radial stresses at each position of the inner ring are all tensile stresses, and the radial tensile stress on the raceway surface is the largest. The second largest radial tensile stress is in the center, while the smallest radial tensile stress is on the inner surface. The stress value at point R3 on the inner ring's raceway is its highest in both the axial and radial directions.

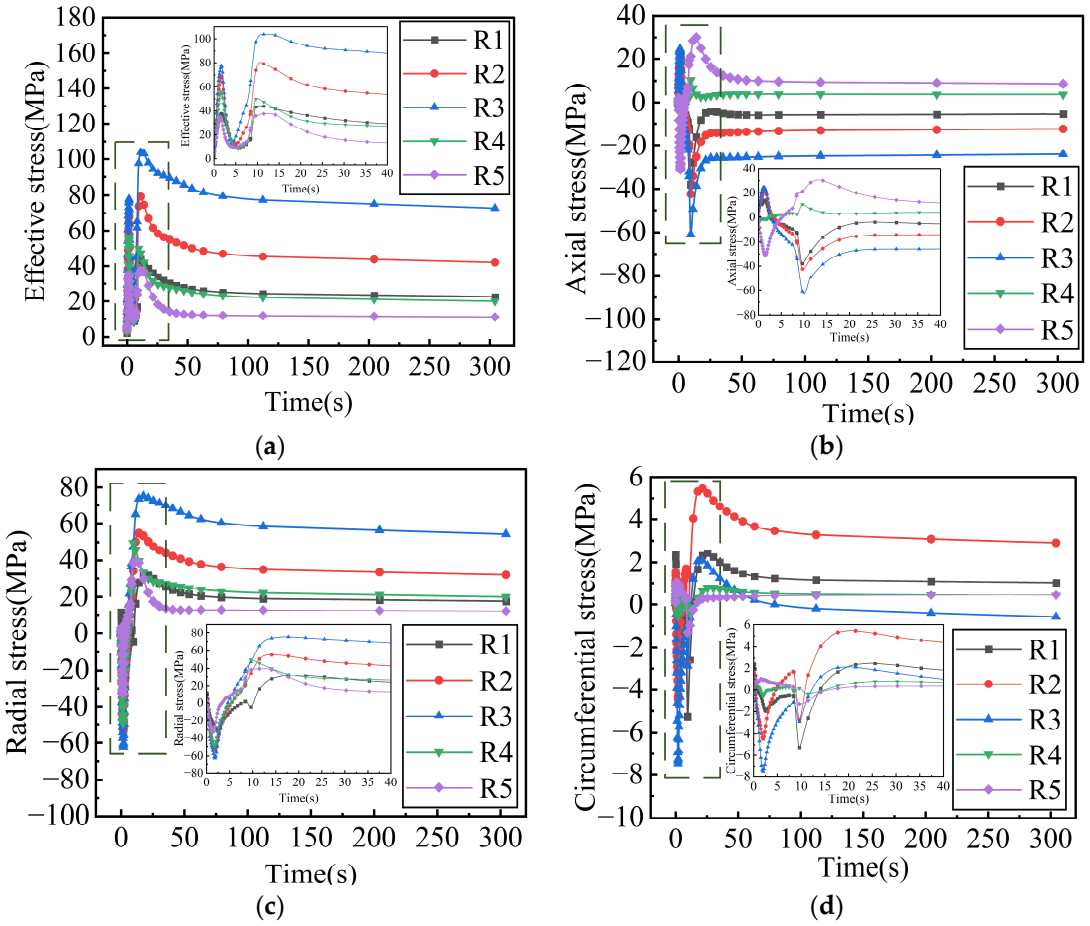


Figure 9. The variation in stress with time during quenching cooling: (**a**) effective stress; (**b**) axial stress; (**c**) radial stress; (**d**) circumferential stress.

4.2. The Deformation of the Bearing Rings During the Quenching Process

4.2.1. The Mechanism of Dimensional Evolution of the Bearing Ring

The dimensional variations in the inner ring during the quenching heating process are shown in Figure 10. As can be seen from Figure 10a, in the initial stage of the heating process, the volume of the inner ring expands due to the effect of high temperatures, and the dimensional variation on the outer surface of the inner ring is larger than that on the inner surface. Additionally, the deformation in the thinner wall is larger than that in the thicker wall. The dimensional variation in the inner ring after the heating process (when the heating time is 736 s) is shown in Figure 10b. At this point, the deformation of the inner ring is larger than that in the initial stage of heating. The dimensional variation in the inner ring at the end of the heating process is shown in Figure 10c. The maximum deformation of the inner ring occurs on the outer surface where the wall thickness is thin, with a value of about 0.298 mm. The minimum deformation of the inner ring occurs on the inner surface where the wall thickness is thicker, with a value of about 0.195 mm. From the dimensional variation cloud diagram, it can be observed that the inner ring exhibits uneven deformation during the heating process.

The dimensional variations during the quenching heating process of the outer ring are shown in Figure 11. From Figure 11a,b, it can be observed that the volume of the outer ring increases due to the high temperatures during the heating process. Due to the thin wall thickness of the outer ring and uneven heating at different locations, uneven deformation occurs. The dimensional variation in the outer ring at the end of heating is shown in Figure 11c. The maximum deformation of the outer ring occurs on the outer surface, and is

about 0.428 mm. The minimum deformation of the outer ring occurs on the inner surface, and is about 0.249 mm.

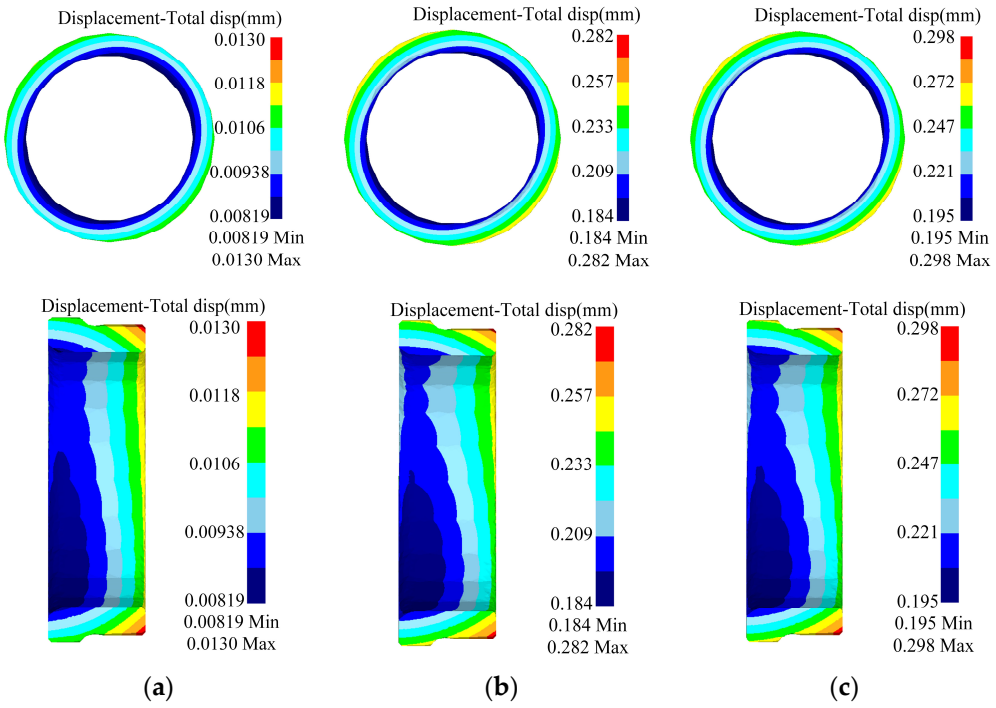


Figure 10. The dimensional variation during the quenching heating process of the inner ring: (**a**) a heating time of 5 s; (**b**) a heating time of 736 s; (**c**) at the end of the heating process.

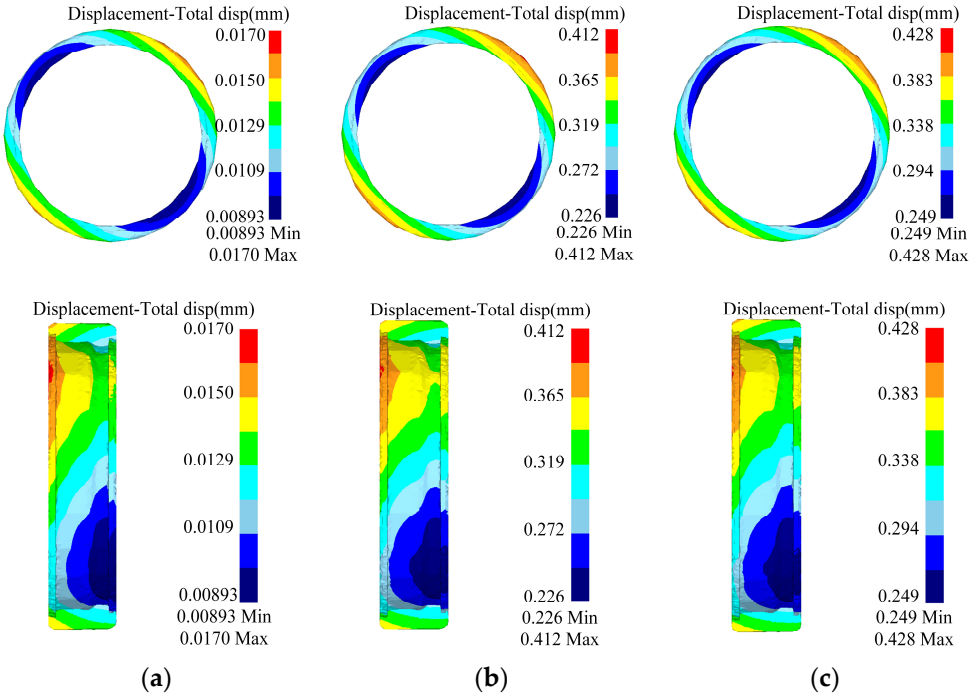


Figure 11. The dimensional variation during the quenching heating process of the outer ring: (**a**) a heating time of 5 s; (**b**) a heating time of 736 s; (**c**) at the end of the heating process.

To further study the dimensional variation in the bearing rings during the heating process, the inner ring was taken as an example, and three nodes were selected, as shown in Figure 12a. The effects of temperature variation and phase transformation on the dimensional variation in the inner ring were explored. The dimensional variation curves of

the inner ring during the quenching heating process are shown in Figure 12b. The volume of the inner ring expands during the quenching process. The largest dimensional increase is observed at point P2 on the outer surface of the inner ring, the second largest increase is at point P1 in the center, and the smallest increase in dimension occurs at point P3 on the inner surface. The increase in the radial dimension at point P2 at the end of the heating process is about 0.25 mm. The variation curves of the microstructure and dimension with heating during the heating process at point P1 of the inner ring are shown in Figure 12c. It can be seen that in the initial stage of the heating process, the volume of the inner ring expands due to high temperatures, and the radial dimension increases. Later, the temperature of the inner ring reaches the austenite phase transition temperature, and austenite transformation occurs. The volume of the inner ring contracts, and the radial dimension decreases. Once the austenite transformation is complete, the radial dimension of the inner ring increases. This is because the inner ring continues to be heated, and its volume continues to expand.

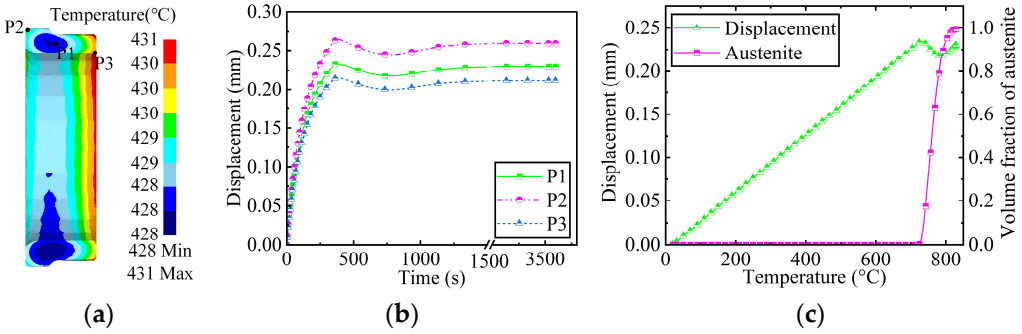


Figure 12. The dimensional variation during the quenching heating process of the inner ring: (**a**) A schematic diagram of the nodes; (**b**) The dimensional variation curve of the inner ring during the heating process; (**c**) The variation curve of the microstructure and dimension with temperature during the heating process at point P1.

The dimensional variations during the quenching cooling process of the inner ring are shown in Figure 13. In Figure 13a, it can be observed that in the initial stage of the quenching cooling process, the heat exchange between the inner ring surface and the quenching oil is intense, causing the volume of the inner ring to decrease. Compared to the dimensional variation in the inner ring at the end of the quenching heating process, the reduction in the dimensions of the outer surface of the inner ring is larger than that of the inner surface during the initial stage of cooling. As shown in Figure 13b,c, the dimensional variation in the inner ring when it is cooled to 14 s is less than the dimensional variation at the end of cooling process. Before 14 s, the dimensional variation in the inner ring is mainly affected by temperature, and its dimension decreases. Afterwards, the temperature of the inner ring reaches the martensite phase transition temperature, and martensite transformation occurs. At this time, the volume of the inner ring expands, and its dimension increases.

The dimensional variations during the quench cooling process of the outer ring are shown in Figure 14. It can be observed that the outer ring exhibits uneven deformation during the cooling process. As shown in Figure 14a, in the initial stage of the cooling process, the temperature of the outer ring rapidly decreases. The volume of the outer ring contracts, and the dimension at each position decreases. The dimensional variation ub the outer ring at 14 s of the cooling process is shown in Figure 14b. The values of dimensional variation at this time are smaller compared to those at the end of the cooling process. This is due to the fact that martensitic phase transformation occurred after 14 s of the cooling process, resulting in the volume of the outer ring expanding. From Figure 14c, it can be seen that at the end of the cooling process, the maximum displacement of the outer ring is

about 0.110 mm on the outer surface and the minimum displacement is about 0.0797 mm on the inner surface.

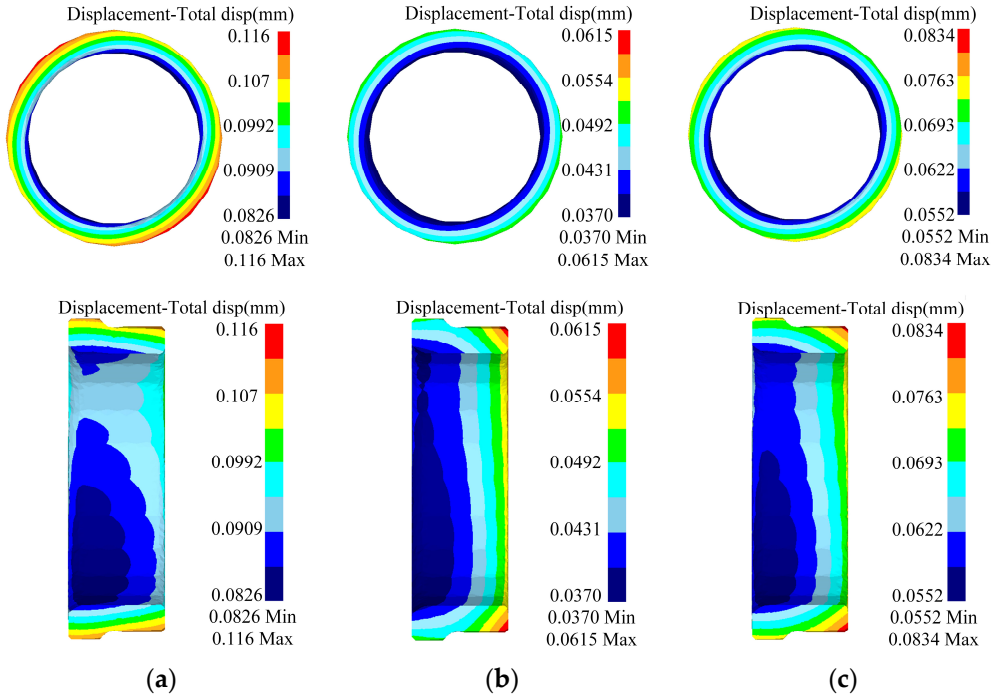


Figure 13. The dimensional variations during the quenching cooling process of the inner ring: (**a**) a cooling time of 3 s; (**b**) a cooling time of 14 s; (**c**) the end of cooling.

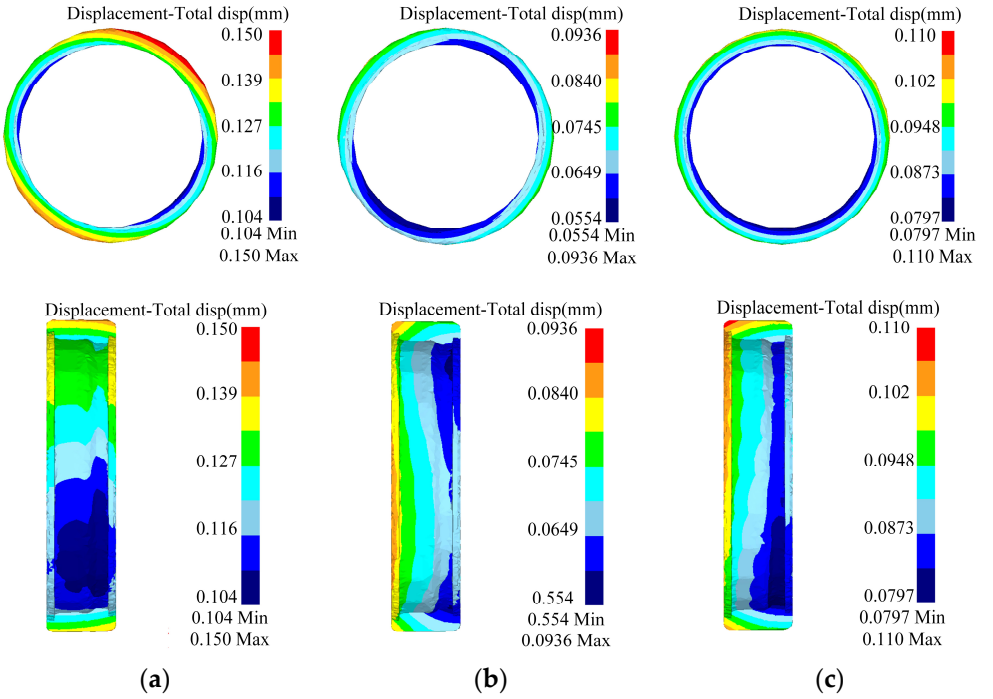


Figure 14. The dimensional variations during the quenching cooling process of the outer ring: (**a**) a cooling time of 3 s; (**b**) a cooling time of 14 s; (**c**) the end of cooling.

To further study the dimensional variation in the bearing rings during the quenching cooling process, the inner ring was taken as an example, as shown in Figure 15a, and three nodes were selected. The effects of temperature variation and phase transformation on the dimensional variation in the inner ring were explored. The dimensional variation curves of the inner ring during the quench cooling process are shown in Figure 15b. During the

cooling process, the radial dimension reduction rate at point P2 on the outer surface of the inner ring is the fastest, followed by point P1 at the center, and point P3 on the inner surface is the slowest. Figure 15c shows the variation curve of microstructure and dimension with temperature during the cooling process at point P1 of the inner ring. Initially, the temperature of the inner ring decreases during the cooling process, and the radial dimension decreases. When the temperature of the inner ring reaches the martensite phase transition temperature, martensite transformation occurs. At this point, the volume of the inner ring expands, and the dimension increases. The extent of austenite to martensite transformation decreases as the martensitic phase transformation approaches completion. The effect of low temperatures on volume reduction is greater than the effect of phase transformation on volume expansion, causing the radial size of the inner ring to decrease. Afterwards, when the temperature of the inner ring reaches the temperature of the quenching medium, the radial dimension no longer changes. The research by Liu [29] and Wang et al. [30] indicated that deformation during the quenching process is mainly the result of the combined effect of phase transformation stress and thermal stress. This is consistent with the findings of this paper.

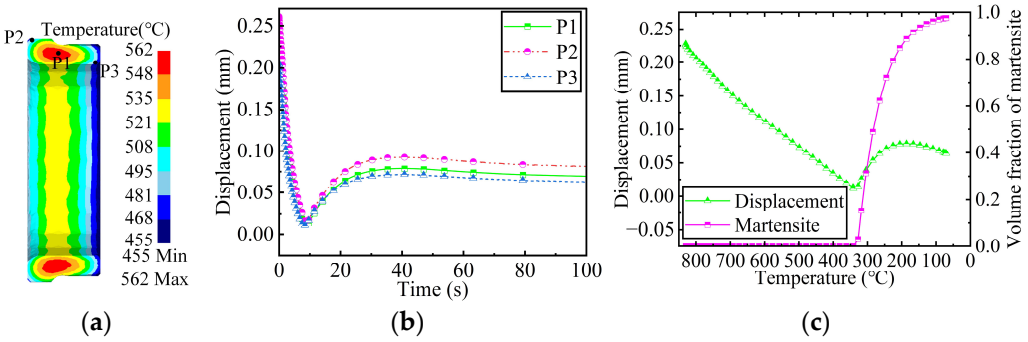


Figure 15. The dimensional variation during the quenching cooling process of the inner ring: (**a**) The schematic diagram of nodes; (**b**) The dimensional variation curve of the inner ring during the cooling process; (**c**) The variation curve of microstructure and dimension with temperature during the cooling process at point P1.

4.2.2. The Experimental Results Are Compared with the Simulation Results

The simulation results of the bearing ring dimensions after quenching and tempering are presented in Figure 16. The difference between the maximum measurement radius and the minimum measurement radius is taken as the roundness error. The simulation results of the inner and outer diameters of the inner ring are shown in Figure 16a,b. The calculated roundness error for the inner diameter is 0.0386 mm, and the roundness error for the outer diameter is 0.0423 mm. The simulation results for the inner and outer diameters of the outer ring are shown in Figure 16c,d. The calculated roundness error for the inner diameter is 0.0202 mm, and the roundness error for the outer diameter is 0.0180 mm.

The measurement results for the roundness of the bearing rings are shown in Figure 17. There is a significant difference in roundness between the different bearing rings. Therefore, three sets of bearing rings were selected to measure their roundness, and the average value of the measurement results was taken as the experimental result. As shown in Figure 17a,b, it can be seen that the errors between the simulation results and the experimental results are within 14% and 17% for the inner and outer rings, respectively.

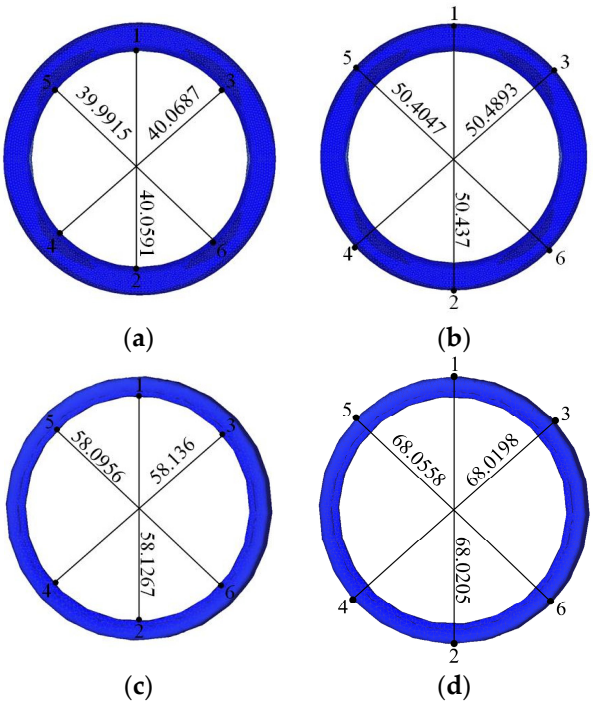


Figure 16. The simulation results for the dimension of the bearing rings after the quenching and tempering processes: (**a**) the roundness of the inner diameter of the inner ring; (**b**) the roundness of the outer diameter of the inner ring; (**c**) the roundness of the inner diameter of the outer ring; (**d**) the roundness of the outer diameter of the outer ring.

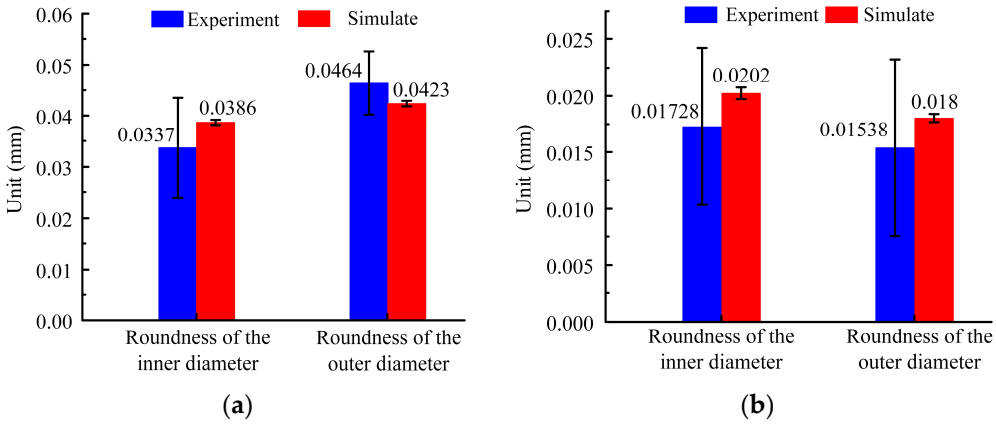


Figure 17. The experimental results are compared with the simulation results: (**a**) the roundness error of the inner ring; (**b**) the roundness error of the outer ring.

5. Conclusions

The rings of angular contact ball bearings (7008C) were selected as the subject of this study. A numerical simulation method was employed to systematically investigate the stress evolution mechanism during the quenching and tempering processes. The effects of temperature variation and phase transformation on the deformation of bearing rings were studied and experimentally verified to assess the accuracy of the simulation results. The following conclusions were drawn:

(1) At the end of the quenching cooling process for the inner ring, the maximum effective stress on the raceway surface was approximately 80 MPa, the axial compressive stress was approximately 30 MPa, and the radial tensile stress was approximately 60 MPa; the maximum effective stress on the inner surface was approximately 18 MPa, the axial tensile stress was approximately 5 MPa, and the radial tensile stress was about 10 MPa;

and the maximum effective stress in the center was approximately 22 MPa, the axial tensile stress was approximately 10 MPa, and the radial tensile stress was approximately 3 MPa.

(2) Both the experimental and simulation results indicate that the uneven expansion and deformation of the bearing rings occurred during the quenching and tempering processes. After the quenching heating process, the maximum displacements of the inner and outer rings were 0.298 mm and 0.428 mm, respectively. Following the quenching cooling process, the maximum displacements of the inner and outer rings were 0.0834 mm and 0.110 mm, respectively.

(3) The bearing rings exhibit uneven expansion deformation after the quenching and tempering processes. The roundness errors for the inner and outer diameters of the inner ring were 0.0386 mm and 0.0423 mm, respectively. The roundness errors for the inner and outer diameters of the outer ring were 0.0202 mm and 0.0180 mm, respectively. The discrepancy between the simulation and experimental results was within 14% for the inner ring and 17% for the outer ring. This shows that the coupled simulation model has high reliability.

(4) During the design of the bearings, the minimum machining allowances for the inner and outer rings can be determined based on the simulation results to reduce production costs. In the production process, to control the roundness error of the bearing rings due to deformation during the heat treatment process, a large number of simulations can be conducted to optimize the heat treatment process parameters.

Author Contributions: Conceptualization, R.G.; Data curation, Y.T. and Q.W.; Funding acquisition, R.G.; Methodology, Y.T.; Project administration, R.G.; Software, Y.T. and Q.W.; Supervision, R.G.; Validation, L.C.; Visualization, Z.S.; Writing–original draft, Y.T.; Writing–review and editing, Q.W. and L.C. All authors have read and agreed to the published version of the manuscript.

Funding: This research was funded by the Ministry of Industry and Information Technology Special Projects (TC220H05V-W03), Henan Provincial Department of Science and Technology (231111221000) and Longmen Laboratory Project (LMQYTSKT036).

Data Availability Statement: All data generated or analyzed during this study are included in this published article.

Conflicts of Interest: The authors declare no conflicts of interest.

References

1. Vencl, A.; Gasic, V.; Stojanovic, B. Fault tree analysis of most common rolling bearing tribological failures. *IOP Conf. Ser. Mater. Sci. Eng.* **2017**, *174*, 1. [CrossRef]
2. Pastukhov, A.; Timashov, E. Procedure for Simulation of Stable Thermal Conductivity of Bearing Assemblies. *Adv. Eng. Lett.* **2023**, *2*, 58–63. [CrossRef]
3. Pastukhov, A.; Timashov, E.; Stanojevic, D. Temperature Conditions and Diagnostics of Bearings. *Adv. Eng. Lett.* **2023**, *8*, 45–51. [CrossRef]
4. Du, F.; Zhou, P.; Gou, P.; Li, C.; Deng, L.; Wang, X.Y.; Jin, J.S. Effect of hot deformation parameters on heat-treated microstructures and mechanical properties of 300M steel. *Materials* **2022**, *15*, 8927. [CrossRef] [PubMed]
5. Ye, X.J.; Yang, B.B.; Liu, J.T.; Li, Y.P. Correlation between microstructure and mechanical properties of heat-treated novel powder metallurgy superalloy. *Materials* **2022**, *15*, 4524. [CrossRef]
6. Wang, F.L.; Ye, X.Y.; Ren, S.B.; Zhang, K.H.; Liang, X.K.; Liu, G. Effect of intercritical annealing time on microstructure evolution and mechanical properties of low carbon medium manganese steel subjected to multi-step heat treatment process. *Materials* **2022**, *15*, 2425. [CrossRef] [PubMed]
7. Kang, H.; Feng, G.Z.; Liu, N. Microstructure and properties of U75V 60 kg/m heavy rail at different cooling rates of heat treatment. *J. Phys. Conf. Ser.* **2023**, *2566*, 1–7. [CrossRef]
8. Yamamoto, T.; Kumagai, K. Effects of Heat-treated Structures and Cold Working on Machinability of Chromium Case-hardening Steels in Comparison with Other Carbon and Low Alloy Steels. *Trans. Iron Steel Inst. Jpn.* **2019**, *15*, 345–352. [CrossRef]

9. Lopez-Garcia, R.D.; Garcia-Pastor, F.A.; Maldonado-Reyes, A.; Jimemez-Gomez, M.A.; Rodriguez-Garcia, J.A. Analysis of the effect of immersion rate on the distortion and residual stresses in quenched SAE 5160 steel using FEM. *J. Mater. Res. Technol.* **2019**, *8*, 5557–5571. [CrossRef]
10. Lopez-Garcia, R.D.; Medina-Juarez, I.; Maldonado-Reyes, A. Effect of Quenching Parameters on Distortion Phenomena in AISI 4340 Steel. *Materials* **2022**, *12*, 759. [CrossRef]
11. Kim, N.K.; Bae, K.Y. Analysis of Deformation in the Carburizing-Quenching Heat Treatment of Helical Gears made of SCM415H Steel. *Int. J. Precis. Eng. Manuf.* **2015**, *16*, 73–79. [CrossRef]
12. Shao, Y.Y.; Peng, W.F.; Chen, S.Q. Effect of cold treatment process on roundness of bearing ring. *Mater. Res. Express* **2022**, *9*, 6513. [CrossRef]
13. Liu, H.M.; Zhao, J.Y.; Tang, J.Y.; Shao, W.; Sun, B.E. Simulation and Experimental Verification of Die Quenching Deformation of Aviation Carburized Face Gear. *Materials* **2023**, *16*, 690. [CrossRef]
14. Liu, J.; Li, J.D.; Tian, Y.; Li, Y.; Wang, Z.D. Effects of vacuum oil quenching on distortion of 42CrMo Navy C-ring. *Mater. Sci. Technol.* **2022**, *38*, 1659–1666. [CrossRef]
15. Li, X.; Ju, D.; Cao, J.; Ishikawa, K. Analysis of the Distortion of the Bearing Rings after Quenching. *Coatings* **2023**, *13*, 1190. [CrossRef]
16. Esfahania, A.K.; Babaeib, M.; Sarrami-Foroushani, S. A numerical model coupling phase transformation to predict microstructure evolution and residual stress during quenching of 1045 steel. *Math. Comput. Simul.* **2021**, *179*, 1–22. [CrossRef]
17. Wang, X.; Li, D.Q.; Li, P. Analysis and Optimization of Carburizing–Quenching Distortion on Locomotive Gear Ring. *JOM* **2023**, *75*, 2441–2450. [CrossRef]
18. Liu, Q.; Ju, D.Y.; Li, X.S.; Ishikawa, K.; Lv, R.; Lian, W.F.; Zhang, M. Verification of the Non-Axisymmetric Deformation Mechanism of Bearing Rings after Quenched in a Multi-Field Coupled Simulation. *Coatings* **2022**, *5*, 676. [CrossRef]
19. Chen, X.J.; Zhang, S.H.; Rolfe, B.; Li, D.Z. The FEM simulation and experiment of quenching distortion of a U-shape sample and the sensitivity analysis of material properties. *Mater. Res. Express* **2019**, *11*, 116539. [CrossRef]
20. Zhang, K.Y.; Dong, W.C.; Lu, S.P. Experimental and Numerical Investigation of Stress and Distortion in AF1410 Steel Under Varying Quenching Conditions. *J. Mater. Eng. Perform.* **2022**, *31*, 6858–6869. [CrossRef]
21. Yan, Y.M.; Xue, Y.J.; Yu, W.C.; Liu, K.; Wang, M.Q.; Wang, X.M.; Ni, L.Q. Predictions and Experiments on the Distortion of the 20Cr2Ni4A C-ring during Carburizing and Quenching Process. *Materials* **2022**, *15*, 4345. [CrossRef]
22. Lin, J.; Li, D.; Zheng, K.; Liu, X. Experimental and modeling study of the interfacial and convective heat transfer coefficients of 6061 aluminum alloy in hot gas forming. *Int. J. Adv. Manuf. Technol.* **2024**, *135*, 985–996. [CrossRef]
23. Zhang, X.; Li, Z.; Cui, X. Numerical simulation of heat treatment deformation of GCr15 bearing rings. *Bearing* **2020**, *11*, 45–49+69. [CrossRef]
24. Zheng, J.; Zhang, W.; Deng, S. Numerical simulation of induction hardening process and organisational properties of spherical roller bearings. *Trans. Mater. Heat Treat.* **2020**, *41*, 133–141. [CrossRef]
25. Zang, L.; Deng, S.; Zhang, W. Numerical simulation of medium-frequency induction quenching of double-row ball bearings. *Trans. Mater. Heat Treat.* **2018**, *39*, 137–144. [CrossRef]
26. Bo, X. Interpretation of GB/T 18254-2016 "High Carbon Chromium Bearing Steel". *Heat Treat.* **2019**, *34*, 57–60.
27. Zhu, K.; Xiong, B.; Li, X.; Zhang, Y.; Li, Z.; Li, Y.; Wen, K.; Yan, L. Finite element simulation on residual stress during immersion quenching and pre-stretching of Al7055 thick plates. *Mater. Res. Express* **2022**, *9*, 026525. [CrossRef]
28. Qin, S.; Ma, H.; Wang, L. Stress field simulation and its experimental verification of carburizing-quenching process performed on 18CrNiMo7-6 steel. *Mater. Sci.* **2023**, *29*. [CrossRef]
29. Liu, Q.; Liu, Q.; Jiang, J.; Chen, M.; Ju, D. Numerical simulation and experimental study on quenching of high carbon chromium bearing outer ring. *J. Ordnance Equip. Eng.* **2023**, *44*, 78–86. [CrossRef]
30. Wang, R.; Jiang, H.; Shao, W.; Yang, S.; Sun, X.; Cao, J.; Zhen, L. Quenching induced residue stress in M50 steel ring: A FEM simulation. *J. Mater. Res. Technol.* **2023**, *24*, 5298–5308. [CrossRef]

Disclaimer/Publisher's Note: The statements, opinions and data contained in all publications are solely those of the individual author(s) and contributor(s) and not of MDPI and/or the editor(s). MDPI and/or the editor(s) disclaim responsibility for any injury to people or property resulting from any ideas, methods, instructions or products referred to in the content.